APPLIED OPTICS

10.1126/sciadv.1501170

Efficient luminescent solar cells based on tailored mixed-cation perovskites

Dongqin Bi,[1] Wolfgang Tress,[2]* M. Ibrahim Dar,[2,3] Peng Gao,[3] Jingshan Luo,[2] Clémentine Renevier,[2] Kurt Schenk,[4] Antonio Abate,[2] Fabrizio Giordano,[2] Juan-Pablo Correa Baena,[1] Jean-David Decoppet,[2] Shaik Mohammed Zakeeruddin,[2] Mohammad Khaja Nazeeruddin,[3] Michael Grätzel,[2] Anders Hagfeldt[1]

We report on a new metal halide perovskite photovoltaic cell that exhibits both very high solar-to-electric power-conversion efficiency and intense electroluminescence. We produce the perovskite films in a single step from a solution containing a mixture of FAI, PbI_2, MABr, and $PbBr_2$ (where FA stands for formamidinium cations and MA stands for methylammonium cations). Using mesoporous TiO_2 and Spiro-OMeTAD as electron- and hole-specific contacts, respectively, we fabricate perovskite solar cells that achieve a maximum power-conversion efficiency of 20.8% for a PbI_2/FAI molar ratio of 1.05 in the precursor solution. Rietveld analysis of x-ray diffraction data reveals that the excess PbI_2 content incorporated into such a film is about 3 wt %. Time-resolved photoluminescence decay measurements show that the small excess of PbI_2 suppresses nonradiative charge carrier recombination. This in turn augments the external electroluminescence quantum efficiency to values of about 0.5%, a record for perovskite photovoltaics approaching that of the best silicon solar cells. Correspondingly, the open-circuit photovoltage reaches 1.18 V under AM 1.5 sunlight.

INTRODUCTION

Metal halide perovskites of the composition ABX_3 [A = Cs^+, $CH_3NH_3^+$ (MA), or $NH{=}CHNH_3^+$ (FA); B = Pb or Sn; X = Br, I] have recently attracted strong research interest because of their outstanding photovoltaic properties (*1*). The development was triggered by the reports of Kojima *et al.* (*2*) and Im *et al.* (*3*) on liquid electrolyte-based quantum dot solar cells. Adoption of solid-state hole conductor and new deposition techniques (*4*–*8*) boosted the power-conversion efficiency (PCE) from 3% (*2*) to the present record of 20.1% (*8*). The latter was reached with perovskites using mixtures of A and X ions with a general formula of $FA_{1-x}MA_xPb(I_{1-y}Br_y)_3$, pioneered by Pellet *et al.* (*9*) and Jeon *et al.* (*10*).

Although the current PCE of 20.1% is impressive, the open-circuit voltage (V_{OC}) of these solar cells remains below 1.1 V, which is lower than their theoretical V_{OC} limit of 1.32 V (for $MAPbI_3$) in AM 1.5 G sunlight (*11*). The loss of more than 200 mV arises from nonradiative recombination of photogenerated charge carriers and manifests itself in a low external quantum yield ($\lessapprox$0.01%) for electroluminescence measured at a forward bias potential corresponding to V_{OC} (*11*, *12*). Reducing nonradiative recombination would pave the way for higher V_{OC} and PCE values. Recent attempts toward this end used additives such as phenyl-C_{61}-butyric acid methyl ester (PCBM) (*13*), oxygen (*14*), and PbI_2 (*15*–*19*). Cao *et al.* (*19*) maintained unreacted PbI_2 during sequential deposition (*7*) of $MAPbI_3$ on a mesoporous TiO_2 scaffold, causing an increase in V_{OC} of up to 1.036 V (PCE = 9.7%) at a residual PbI_2 level of 1.7%. This was ascribed to elimination of surface states by PbI_2, in agreement with photovoltage spectroscopy measurements that also point to a decrease in $MAPbI_3$ defect states by unreacted PbI_2 (*18*). Similar beneficial effects have been ascribed by Chen *et al.* (*15*) and Pathak *et al.* (*20*) to the surface enrichment of PbI_2 formed by thermal decomposition of $MAPbI_3$. In contrast, Shao *et al.* (*13*) found that such PbI_2-enriched perovskite layers are n-doped and contain a high level of defects that were eliminated by the deposition of a PCBM overlayer. In most of these cases, the influence of excess PbI_2 was studied using devices with poor or moderate performance (PCE $\lessapprox$ 12%). Hence, it appears that it is difficult to attribute these sometimes contradictory effects to the mere presence of excess PbI_2.

RESULTS

Here, we report for the first time on a perovskite solar cell (PSC) using a new PbI_2-enriched composition that exhibits both very high solar-to-electric PCE and intense electroluminescence. We produce the mixed-cation mixed-halide perovskite films in a single step from a solution of FAI, PbI_2, MABr, and $PbBr_2$ in a mixed solvent containing dimethyl formamide (DMF) and dimethyl sulfoxide (DMSO). We vary the molar ratio for PbI_2/FAI ($R_{PbI_2/FAI}$) from 0.85 to 1.54 while maintaining a fixed molar ratio of 5.67 for $PbI_2/PbBr_2$ in the precursor solutions. By using this technique, we fabricate PSC with the structure Au/Spiro-OMeTAD/perovskite/mesoporous TiO_2/compact TiO_2/FTO. We achieve the highest PCE (20.8%) with $R_{PbI_2/FAI} = 1.05$, corresponding to a 3% weight excess of PbI_2 in the perovskite. The photovoltaic metrics of the device are as follows: short-circuit current density (J_{SC}) = 24.6 mA cm^{-2}, open-circuit voltage (V_{OC}) = 1.16 V, and fill factor (FF) = 0.73 (Fig. 1A). By integrating the incident photon-to-electron conversion efficiency (IPCE) spectrum over the AM 1.5 photon flux, we obtain J_{SC} values that agree within 4% of the measured values. One of the devices was sent for certification to Newport Corporation, an accredited photovoltaic testing laboratory, confirming PCEs of 19.90% (backward scan) and 19.73% (forward scan) with a J_{SC} of 23.2 mA cm^{-2} and a V_{OC} of 1.13 V (fig. S1). The normalized IPCE spectrum is shown in fig. S1 as well. The commonly observed hysteresis (*13*, *21*) is not pronounced in our

[1]Laboratory of Photomolecular Science, Ecole Polytechnique Fédérale de Lausanne, Lausanne CH-1015, Switzerland. [2]Laboratory of Photonics and Interfaces, Ecole Polytechnique Fédérale de Lausanne, Lausanne CH-1015, Switzerland. [3]Group for Molecular Engineering of Functional Materials, Ecole Polytechnique Fédérale de Lausanne, Lausanne CH-1015, Switzerland. [4]Institute of Chemical Sciences and Engineering, Ecole Polytechnique Fédérale de Lausanne, Lausanne CH-1015, Switzerland.
*Corresponding author. E-mail: wolfgang.tress@epfl.ch

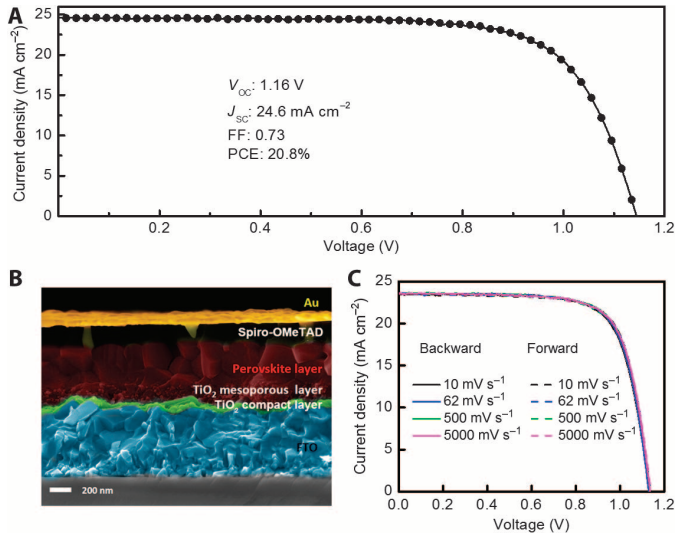

Fig. 1. Basic characteristics of fabricated perovskite solar cells. (**A**) *J-V* curves for the champion solar cell under AM 1.5 G illumination, measured from V_{OC} to J_{SC}. (**B**) Cross-sectional SEM image of the champion cell. (**C**) Hysteresis measurements of one PSC at different scanning speeds under AM 1.5 G illumination.

devices, as proven by *J-V* curves shown in Fig. 1C (table S1), where the voltage sweep rate was varied from 10 to 5000 mV s^{-1}. A cross-sectional scanning electron microscopy (SEM) image of a champion PSC is shown in Fig. 1B, visualizing a thick perovskite capping layer of around 500 nm. A histogram of 40 devices (figs. S2 and S3) indicates good performance reproducibility, with an average PCE of 19.5%. A preliminary stability investigation shows that the devices stored in the dark at room temperature are relatively stable, with a PCE drop of only 0.3% for 1 month (fig. S4 and table S2).

The photovoltaic metrics of the PSCs made by varying $R_{PbI_2/FAI}$ in the precursor solution are summarized in Fig. 2 (A to D). For $R_{PbI_2/FAI} < 1$ or $R_{PbI_2/FAI} > 1.23$, the device performance deteriorates considerably. However, in the range of $R_{PbI_2/FAI} =$ 1–1.16, J_{SC} and FF show a plateau, whereas V_{OC} increases substantially, reaching a maximum of 1.17 V at $R_{PbI_2/FAI} =$ 1.16 (1.18 V without aperture; see discussion in Materials and Methods). This is the highest V_{OC} observed so far for lead iodide–based PSCs on mesoporous TiO_2, resulting in a PCE larger than 19%. During the rise of V_{OC}, J_{SC} maintains a large value (more than 23 mA cm^{-2}) because the band gap does not alter strongly for the different perovskite compositions, as shown by the absorbance spectra in fig. S5. The FF is around 0.72, indicating that a moderate excess of PbI_2 does

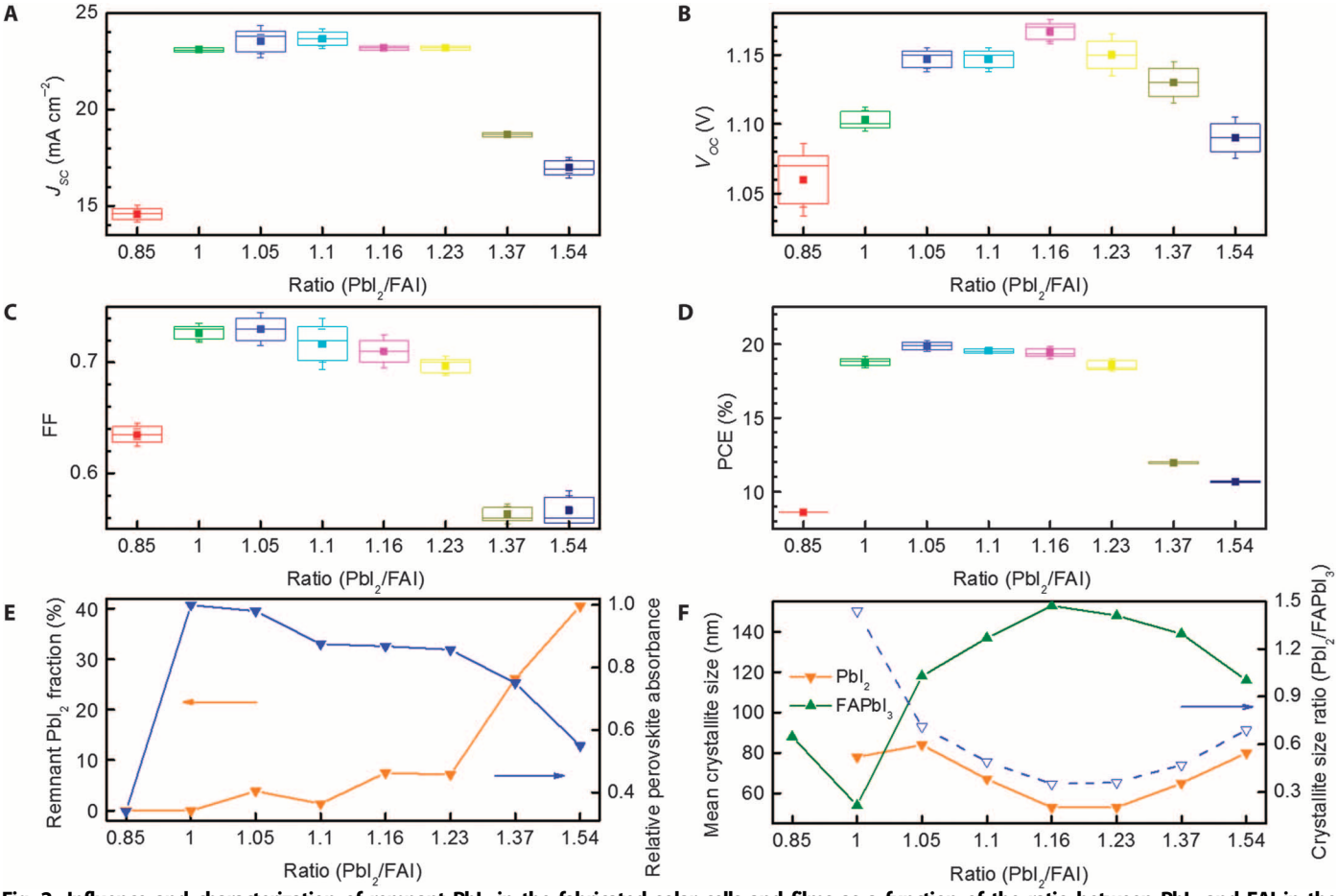

Fig. 2. Influence and characterization of remnant PbI_2 in the fabricated solar cells and films as a function of the ratio between PbI_2 and FAI in the precursor solution. (**A** to **D**) Photovoltaic parameters J_{SC} (A), V_{OC} (B), FF (C), and PCE (D) versus $R_{PbI_2/FAI}$, measured under AM 1.5 G illumination (100 mW cm^{-2}). (**E**) Fraction of remnant PbI_2 (left axis, orange line) and relative perovskite absorbance (right axis, blue line). (**F**) Mean crystallite sizes of $FAPbI_3$ (left axis, green line) and PbI_2 (left axis, orange line) phases determined by Rietveld refinement of thin-film XRD patterns and mean crystallite size ratio of PbI_2/FAI (right axis).

not retard charge collection, which is efficient in these mixed perovskites, allowing for the use of 500-nm capping layers to obtain a sharp IPCE onset and extraordinarily high photocurrents. Thus, overstoichiometric PbI_2 in this range does not strongly influence the composition and optical properties of the perovskite films but improves their electronic quality. This allows for simultaneously high J_{SC} and V_{OC} but avoids the commonly observed "tradeoff" between V_{OC} and J_{SC} when tuning the band gap (*22*, *23*). In the following sections, we quantify and characterize the PbI_2 content remaining in the film. Subsequently, we investigate the role of PbI_2 in reducing nonradiative recombination.

SEM images of perovskite films deposited on a mesoporous TiO_2/compact TiO_2/FTO substrate with varied $R_{PbI_2/FAI}$ are shown in fig. S6. The film morphology changes when $R_{PbI_2/FAI} < 1$ and $R_{PbI_2/FAI} > 1.23$, indicating a modification of the perovskite morphology or the appearance of new phases. To further explore the film composition, we conducted thin-film x-ray diffraction (XRD) measurements for perovskite films deposited again on mesoporous TiO_2/compact TiO_2/FTO substrates (table S3 and figs. S7 and S8). Except for the sample with $R_{PbI_2/FAI} = 0.85$, a peak at 12.5° is observed, which is attributed to the (001) lattice planes of hexagonal (2*H* polytype) PbI_2. The PbI_2 content (Fig. 2E) increases with $R_{PbI_2/FAI}$, showing a 3.8% excess in weight for the most efficient device ($R_{PbI_2/FAI} = 1.05$) and a 7.5% excess in weight for the highest V_{OC} device ($R_{PbI_2/FAI} = 1.16$) (table S1). These values are close to those expected from the molar ratios of the precursors in the spin-coating solution, which correspond to approximately 3 and 10 wt %, respectively. The relative amount of perovskite (Fig. 2E) deduced from absorption measurements shows a reverse trend as compared with the remnant PbI_2 but follows the J_{SC} values (Fig. 2A), indicating that losses in J_{SC} are due to reduced light harvesting rather than reduced charge collection. Because the thicknesses of all perovskite films are similar (fig. S9), the changes in absorbance indicate a significant ratio of nonperovskite material. The opposite trends in the mean crystallite sizes of PbI_2 and perovskite (Fig. 2F) could be due to the competitive expansion of two crystal domains. Coincidentally, the mean crystallite size of the perovskite phase follows the same trend as V_{OC} (shown in Fig. 2B). The trend in the crystallite size ratio of PbI_2 and perovskite (Fig. 2F) mirrors that of V_{OC} and reaches 0.35 for the film with the highest V_{OC}. Thus, excess PbI_2 not only exists as a crystalline phase but also influences the morphology and crystallite size of the perovskite phase. The observed correlation of the open-circuit voltage with the mean crystallite size is likely due to the fact that larger perovskite crystallites exhibit a reduced area of grain boundaries. Consequently, the overall density of defect states is lower.

DISCUSSION

To study the electronic quality of the device and to identify the recombination mechanisms limiting V_{OC}, we performed electroluminescence measurements in which we applied a forward bias to the solar cell in the dark and operated it as a light-emitting diode (LED). Figure 3A contains data for the device ($R_{PbI_2/FAI} = 1.16$), with a V_{OC} of 1.18 V. The blue curve shows injection current versus voltage, where the signature of a shunt for low voltages is followed by an exponential region dominated by recombination in the device. For voltages larger than 1.2 V, limitations by the series resistance become apparent. The red curve shows the emitted photon flux, which increases exponentially with voltage. The diode ideality factor derived from the "slope" is approximately 2 for the current and 1 for the emitted photon flux, indicating that much of the recombination happens through defects [Shockley-Read-Hall (SRH)], whereas emission originates from band-to-band recombination. The external electroluminescence quantum efficiency (EQE_{EL}) increases linearly with injection current (fig. S10), as expected from a device with an ideality factor of 2 (*24*), and approaches 0.5% for currents in the range of J_{SC}. This value translates into a voltage loss of $kT/e \ln(1/EQE_{EL}) = 0.14$ V, confirming the measured $V_{OC} = 1.32\ V - 0.14\ V = 1.18$ V [where 1.32 V is the theoretical maximum V_{OC} (radiative limit)], which we determined for this solar cell using its IPCE action spectrum and following the approach of Tress *et al.* (*11*).

An EQE_{EL} of 0.5% is a record for solution-processed solar cells such as organics, where it is commonly $<10^{-6}$ (*25*), and approaches that of the best silicon solar cells (*26*). Even when compared to perovskite-based LEDs, our EQE_{EL} is among the highest. Our solar cell LED delivers an overall electric power to light conversion efficiency of as high as 0.5% at a voltage of 1.5 V (which is still below E_g/e), whereas reported LEDs show the same efficiency at voltages higher than 3 to 4 V (*27*, *28*). An LED efficiency of 3.5% has been obtained recently, but under much larger charge carrier densities [that is, not under solar cell operating conditions (2.2 V, 160 mA cm^{-2}, and 50-nm layer thickness)] (*29*). Our high EQE_{EL} indicates a high-quality perovskite film and a very good charge selectivity of the contacts, accompanied by a high built-in potential and/or very balanced injection and transport of electrons and holes.

To analyze the dynamics of recombination, we performed time-correlated single photon counting (TCSPC) measurements at different excitation fluences. The photoluminescence (PL) decays for perovskite films with $R_{PbI_2/FAI} = 1$ and $R_{PbI_2/FAI} = 1.16$ deposited on mesoporous TiO_2/compact TiO_2/FTO substrate are shown in Fig. 3 (B and C) (for all samples in figs. S11 and S12).

For the highest light intensity generating approximately $n = 2 \times 10^{17}$ charges per cubic centimeter, the overall decay becomes faster as a result of direct electron-hole recombination, where the recombination coefficient $\beta \approx 2\ldots4 \times 10^{-11}$ $cm^3\ s^{-1}$ in $dn/dt = -\beta n^2 - kn$ describes radiative recombination resulting in the expected V_{OC} of ≈1.3 V (derivation in Materials and Methods). For long time scales or decreased excitation intensity, the PL shows monoexponential decay characteristic of SRH recombination. We deduced 220 and 350 ns, respectively, as nonradiative lifetimes $1/k$ for the two perovskite films with $R_{PbI_2/FAI} = 1$ and $R_{PbI_2/FAI} = 1.16$, consistent with the trend in V_{OC}. In addition, the signal drops strongly in the first few nanoseconds as a result of trap filling. The loss of PL is more significant for the stoichiometric device, in particular when illuminated from the TiO_2 side. This indicates that the trap density is lower for $R_{PbI_2/FAI} = 1.16$ as a result of either a better passivation of traps at the perovskite/TiO_2 interface or a better quality of the perovskite crystallites.

To further elucidate this, we investigate V_{OC} as a function of illumination intensity, represented by J_{SC} in Fig. 3D ($J_{SC} \propto$ intensity). The dashed lines visualizing the theoretical slope for SRH recombination indicate that V_{OC} is mainly limited by SRH recombination. The device with $R_{PbI_2/FAI} = 1.16$ shows a reduced slope toward higher intensities. This is consistent with the bending seen in EQE_{EL} as a function of injection current (fig. S10). Because V_{OC} is still below the radiative limit, this reduced slope is most likely due to losses of charges at a nonperfectly selective contact.

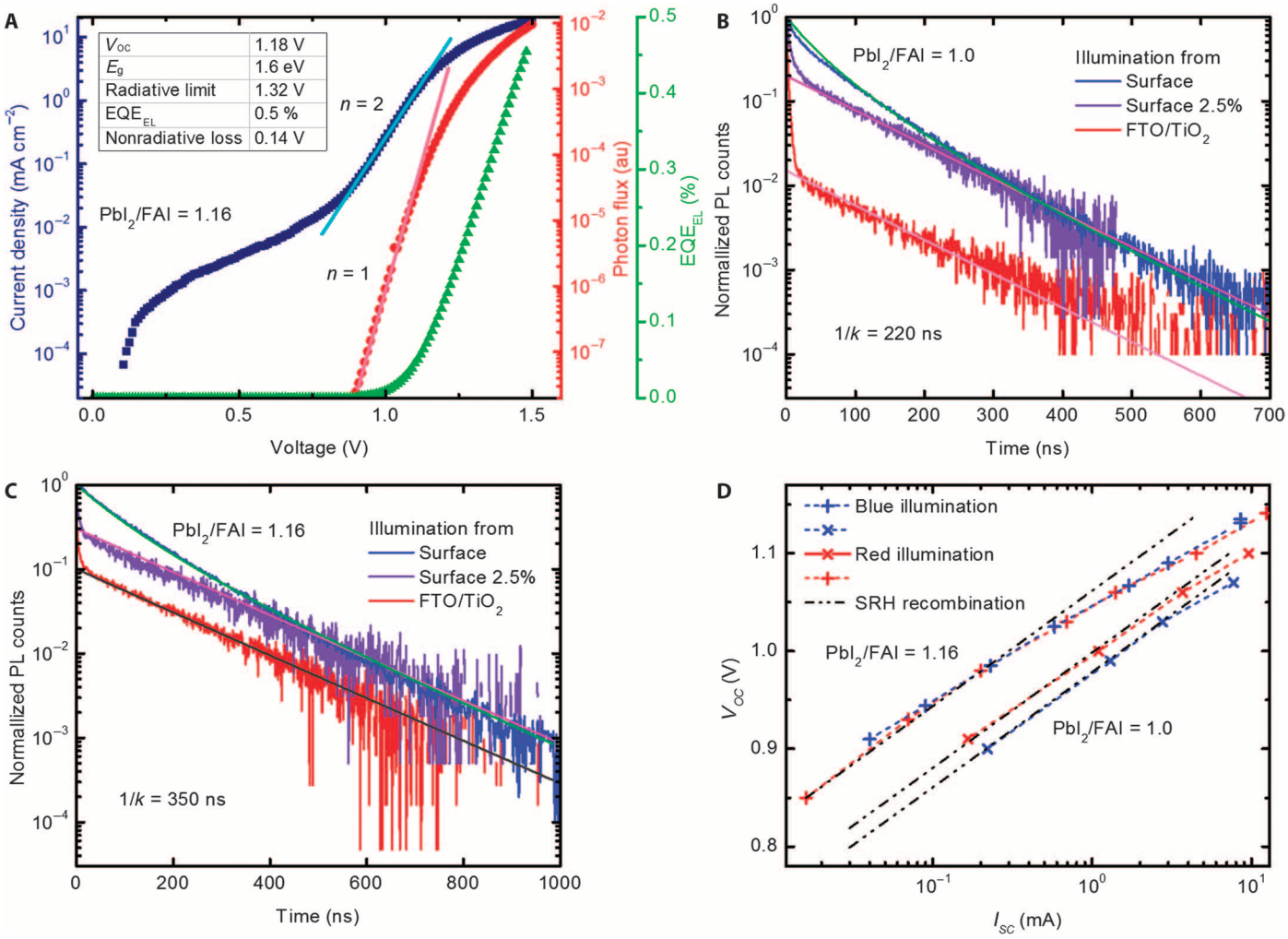

Fig. 3. Characterization of recombination mechanisms and rates. (**A**) Current-voltage curve in the dark (blue), emitted photon flux (red), and external electroluminescence quantum efficiency (EQE_{EL}) (green) of a device with $R_{PbI_2/FAI} = 1.16$. Lines are a guide to the eye, indicating the slopes for an ideality factor of 2 and 1, respectively, assuming a temperature of 320 K. au, arbitrary units. (**B** and **C**) PL decay for a film with $R_{PbI_2/FAI} = 1.0$ and $R_{PbI_2/FAI} = 1.16$. Lines are calculated according to the rate equation in the text. (**D**) V_{OC} as a function of short-circuit current I_{SC} proportional to the light intensity, which was varied for blue and red illuminations.

We use illumination with different wavelengths to tune the absorption profile in the perovskite film. Because of the strong dependence of the absorption coefficient on wavelength (fig. S5), red light (630 nm) and blue light (460 nm) penetrate the film to varied extent: 90% of the blue light is absorbed over a distance <200 nm away from FTO, whereas red light penetrates much farther. Figure 3D shows a significant difference only for the stoichiometric device, where V_{OC} is lower for blue illumination despite the fact that the generated charge carrier density is higher. This is in accordance with the PL decay and proves that this device shows its highest defect density close to TiO_2, the impact of which is reduced in the presence of overstoichiometric PbI_2.

From the PL decay and the monochromatic V_{OC} study, we contend that the role of excess PbI_2 is to reduce recombination close to the perovskite/TiO_2 interface. Thus, PbI_2 crystallites, which are located within the mesoporous TiO_2 scaffold, prevent recombination of holes photogenerated in this region of the absorber. Furthermore, PbI_2 crystallites, which are present within the mesoporous TiO_2 layer, favor the growth of bigger perovskite crystallites, which exhibit a reduced area of grain boundaries and, therefore, fewer defects.

To conclude, we have shown that an excess of PbI_2 of up to ≈8 wt % can enhance the electronic quality of the perovskite/TiO_2 film. With the adoption of this approach, devices based on mixed perovskite enabled a PCE of 20.8% and an open-circuit voltage of 1.18 V, accompanied by a high external electroluminescence quantum efficiency of 0.5%, which is attributed to reduced recombination via defects due to a moderate excess of PbI_2. Further optimization along this path will lead to solution-processed solar cells approaching the theoretical limits for open-circuit voltage and efficiency.

MATERIALS AND METHODS

Materials

All materials were purchased from Sigma-Aldrich and used as received, unless stated otherwise.

Synthesis of inorganic/organic halide materials

$NH{=}CHNH_3I$ was synthesized by slowly dropping 15 ml of hydroiodic acid (45 wt % in water) (Applichem) to a solution of 5 g of formamidine acetate in methanol cooled at 0°C. The solution was further stirred for 5 hours at room temperature. The light-yellow solution was concentrated by rotary evaporation at 80°C until no obvious liquid remained. The crude solid was then dissolved by a minimum amount of methanol, reprecipitated in diethyl ether, and filtered. The procedure was repeated three times, and the resulting white solid was collected and dried at 80°C under vacuum for 2 days: ^{1}H nuclear magnetic resonance (DMSO-d_6) δ 8.76 (s, 4*H*), 7.85 (s, 1*H*) ppm; ^{13}C nuclear magnetic resonance (DMSO-d_6) δ 157.05 ppm.

CH_3NH_3Br was synthesized by slowly dropping 31.1 ml of hydrobromide acid (48 wt % in water) (Fluka) to a solution of 27.86 ml of CH_3NH_2 (40 wt % solution in absolute methanol; TCI) cooled at 0°C. The solution was further stirred for 5 hours at room temperature. The colorless solution was concentrated by rotary evaporation at 50°C until no obvious liquid remained. The crude solid was then dissolved by a minimum amount of ethanol, reprecipitated in diethyl ether, and filtered. The procedure was repeated three times, and the resulting white solid was collected and dried at room temperature under vacuum for 2 days.

Solar cell preparation

The fluorine-doped tin oxide–coated glass (NSG) was sequentially cleaned using detergent, acetone, and ethanol. A 20- to 30-nm TiO_2 blocking layer was deposited on the cleaned FTO by spray pyrolysis, using O_2 as carrier gas, at 450°C from a precursor solution of 0.6 ml of titanium diisopropoxide and 0.4 ml of bis(acetylacetonate) in 7 ml of anhydrous isopropanol. A 200-nm mesoporous TiO_2 was coated on the substrate by spin coating at a speed of 4500 rpm for 15 s with a ramp-up of 2000 rpm s^{-1} from a diluted 30-nm particle paste (Dyesol) in ethanol; the weight ratio of TiO_2 (Dyesol paste) to ethanol is 5.5:1. After spin coating, the substrate was immediately dried on a hotplate at 80°C, and the substrates were then sintered at 500°C for 20 min. The perovskite film was deposited by spin coating onto the TiO_2 substrate. The precursor solution was prepared in a glovebox of 1.35 M Pb^{2+} (PbI_2 and $PbBr_2$) in a mixed solvent of DMF and DMSO; the volume ratio of DMF to DMSO was 4:1. The molar ratio for PbI_2 (specified purity >98%; TCI)/$PbBr_2$(purity, 99.999%; Alfa Aesar) was fixed at 0.85:0.15, and the molar ratio for MABr/$PbBr_2$ was fixed at 1:1. A comprehensive analysis carried out by an analytical institution and covering more than 70 elements showed that the purity of the TCI product (PbI_2) exceeded 99.99%. Thus, it was much purer than specified, implying that changes in molar ratio within the range of some percentages in the precursor solutions are not superimposed by the effects of impurities.

By changing the amount of FAI, we obtained different molar ratios for PbI_2/FAI varying from 1.54 to 1.37, 1.23, 1.16, 1.10, 1.05, 1.00, and 0.85. The spin-coating procedure was performed in an argon flowing glovebox: first, 2000 rpm for 10 s with a ramp-up of 200 rpm s^{-1}; second, 6000 rpm for 30 s with a ramp-up of 2000 rpm s^{-1}. Chlorobenzene (110 μl) was dropped on the spinning substrate during the second spin-coating step 20 s before the end of the procedure. The substrate was then heated at 100°C for 90 min on a hotplate. After cooling down to room temperature, Spiro-OMeTAD (Merck) was subsequently deposited on top of the perovskite layer by spin coating at 3000 rpm for 20 s. The Spiro-OMeTAD solution was prepared by dissolving Spiro-OMeTAD in chlorobenzene (60 mM), with the addition of 30 mM bis(trifluoromethanesulfonyl)imide (from a stock solution in acetonitrile) and 200 mM *tert*-butylpyridine. Finally, FK209 [tris(2-(1*H*-pyrazol-1-yl)-4-*tert*-butylpyridine)-cobalt(III) tris(bis(trifluoromethylsulfonyl)imide); Dyenamo AB] was added to the Spiro-OMeTAD solution (from a stock solution in acetonitrile); the molar ratio for FK209 and Spiro-OMeTAD was 0.03. Finally, 80 nm of gold was deposited by thermal evaporation using a shadow mask to pattern the electrodes.

Characterization

Current-voltage characteristics were recorded by applying an external potential bias to the cell while recording the generated photocurrent with a digital source meter (Keithley model 2400). The light source was a 450-W xenon lamp (Oriel) equipped with a Schott K113 Tempax sunlight filter (Praezisions Glas & Optik GmbH) to match the emission spectrum of the lamp with the AM 1.5 G standard. Before each measurement, the exact light intensity was determined using a calibrated Si reference diode equipped with an infrared cutoff filter (Schott KG-3).

To specify the illuminated area, we used an aperture (shadow mask) with an area of 0.16 cm^2, whereas the total device area defined by the overlap of the electrodes was approximately 0.36 cm^2. This approach allows for an accurate determination of the short-circuit current density but has drawbacks when determining the open-circuit voltage (V_{OC}) as V_{OC} depends on the dark current flowing through the device according to the equation: $V_{OC} = n_{ID}kT/e \ln(I_{SC}/I_0 + 1)$. If there is a mismatch between the illuminated area and the dark area, the ratio between the photocurrent I_{SC} and the dark saturation current I_0 is artificially changed by this ratio. Therefore, the open-circuit voltage was additionally measured without aperture.

XRD spectra were recorded on an X'Pert MPD PRO (PANalytical) equipped with a ceramic tube providing Ni-filtered (CuKα, λ = 1.54060 Å) radiation and on an RTMS X'Celerator (PANalytical). The measurements were performed in Bragg-Brentano geometry 2θ = 8° to 88°. The samples were mounted without further modification, and the automatic divergence slit (10 mm) and beam mask (10 mm) were adjusted to the dimension of the films. A step size of 0.008° was chosen for an acquisition time of 270.57 s deg^{-1}. A baseline correction was applied to all x-ray thin-film diffractograms to compensate for the broad feature arising from the FTO glass and anatase substrate. The presence of strong thermal diffuse scattering and turbostratic disorder, mainly in the PbI_2 films, thwarted a successful Rietveld refinement of up to six phases. Finally, the areas of the (001) maximum of PbI_2 and the (011)/(101) peaks of $FAPbI_3$, calculated by means of a pseudo-Voigt function, were used to estimate the weight fractions. These pseudo-Voigt functions also furnished the full widths at half maximum, which were subsequently used to compute the sizes of the coherent domains along the diffraction vectors by means of Scherrer's equation, setting $K = 1$. SEM images were recorded using a high-resolution scanning electron microscope (Zeiss Merlin).

Electroluminescence yield. The emitted photon flux was detected with a large-area (1 cm^2) Si-photodiode (Hamamatsu S1227-1010BQ) positioned close to the sample. Because of the nonconsidered angular dependence of emission and detector sensitivity, EQE_{EL} was expected to be slightly underestimated (on the order of 10%). The driving voltage was applied using a Bio-Logic SP300 potentiostat, which was also used to measure the short-circuit current of the detector at a second channel.

Absorption spectra were measured on a PerkinElmer ultraviolet (UV)–vis spectrophotometer. Absorbance was determined from a transmittance measurement using an integrating sphere. We used the "PerkinElmer Lambda 950 nm" setup with the integrating sphere system "60 nm InGaAs integrating sphere." The sources were deuterium and tungsten halogen lamps, and the signal was detected by a gridless photomultiplier with Peltier-controlled PbS detector. The UV WinLab software was used to process the data.

PL and TCSPC experiments. PL spectra were recorded by exciting the perovskite films deposited onto mesoporous TiO_2 at 460 nm with a standard 450-W Xenon CW lamp. The signal was recorded with a spectrofluorometer (Fluorolog; Horiba Jobin Yvon Technology FL1065) and analyzed with the software FluorEssence.

The PL decay experiments were performed on the same samples using the same Fluorolog with a pulsed source at 406 nm (Horiba NanoLED 402-LH; pulse width <200 ps, 11 pJ per pulse, approximately 1 mm^2 in spot size), and the signal was recorded using TCSPC. The samples were excited from the perovskite and glass side under ambient conditions.

Analysis of the PL decay. From the pump fluence, we estimated an initial photogenerated charge carrier density on the order of 2×10^{17} cm^{-3} upon excitation at the highest intensity. For a filter with a transmittance of 2.5%, we expected 5×10^{15} cm^{-3}. Assuming that most of the charge carriers in the perovskite are photogenerated (that is, the intrinsic charge carrier density is low), we can set the electron density equal to the hole density and write the continuity equation for photogenerated electrons: $dn/dt = -\beta n^2 - kn$, assuming that changes in the charge density n are due to either a bimolecular process or monomolecular recombination. Solving this equation for $n(t)$ and assuming that the PL signal is proportional to $n^2(t)$, we can calculate the PL decay (solid lines in the main paper).

The ideal solar cell without nonradiative recombination should have $k = 0$. Then, V_{OC} can be calculated, assuming that the charge carrier generation rate G equals the recombination rate R: $G = R = \beta n^2$. For a semiconductor using Boltzmann statistics and effective mass approximation, V_{OC} can be written as $eV_{OC} = E_g - kT \ln(N_c N_v / np)$, with the effective densities of states in conduction and valence band: $N_{c,v} = 2 \times (2\pi m_{e,h}^* k_B T/h^2)^{3/2}$. Thus, knowing the effective mass $m_{e,h}$, temperature T, β, band gap E_g, and light intensity, V_{OC} can be calculated as $V_{OC} = E_g/e - kT/e \ln(N_c N_v \beta/G) \approx 1.3$ V, where we approximated $G = J_{SC}/(e \times \text{thickness}) = 3 \times 10^{27}$ m^{-3} s^{-1}. This is a rough estimation where the order of magnitude of the input parameters—but not their exact values—is known. Effective masses have been taken from Giorgi *et al.* (*30*).

SUPPLEMENTARY MATERIALS

Supplementary material for this article is available at http://advances.sciencemag.org/cgi/content/full/2/1/e1501170/DC1

Fig. S1. Independent certification from Newport Corporation confirming PCEs of 19.90% (backward scan) and 19.73% (forward scan) and a normalized electroluminescence quantum efficiency.

Fig. S2. Photograph of two real devices (front view and back view) showing the active area of the solar cell, the high reflectivity of the smooth gold electrode, and the densely opaque optical appearance of the perovskite film.

Fig. S3. Histogram of solar cell efficiencies for 40 solar cells, with the optimized PbI_2/FAI = 1.05.

Fig. S4. Initial stability test of PSCs sealed using epoxy and stored in a desiccator in the dark.

Fig. S5. Absorption spectra of perovskite films on m-TiO_2/c-TiO_2/FTO substrate with varying $R_{PbI_2/FAI}$ measured in transmission.

Fig. S6. Top-view SEM images of perovskite films on ms-TiO_2/c-TiO_2/FTO with varying PbI_2/FAI ratios (0.85, 1, 1.05, 1.1, 1.16, 1.23, 1.37, and 1.54) in the precursor solutions.

Fig. S7. XRD patterns of perovskite films on ms-TiO_2/c-TiO_2/FTO with varying PbI_2/FAI ratios (0.85, 1, 1.05, 1.1, 1.16, 1.23, 1.37, and 1.54) in the precursor solutions.

Fig. S8. Normalized (001) peaks of PbI_2 phase showing the variation in full widths at half maximum with increasing ratios of PbI_2/$FAPbI_3$ fraction.

Fig. S9. Cross-sectional SEM images of perovskite films on ms-TiO_2/c-TiO_2/FTO with varying PbI_2/FAI ratios (1, 1.05, 1.1, 1.23, 1.37, and 1.54) in the precursor solution.

Fig. S10. External electroluminescence quantum efficiency as a function of the injection current for the device with PbI_2/FAI = 1.16.

Fig. S11. Normalized PL spectra of perovskite films on ms-TiO_2/bl-TiO_2/FTO with varying PbI_2/FAI ratios (1, 1.05, 1.1, 1.23, 1.37, and 1.54) in the precursor solution.

Fig. S12. PL decay of perovskite films on ms-TiO_2/bl-TiO_2/FTO with varying PbI_2/FAI ratios (1, 1.05, 1.1, 1.16, 1.23, 1.37, and 1.54) in the precursor solution.

Table S1. Photovoltaic parameters for PSCs measured using forward scan (from J_{SC} to V_{OC}) and backward scan (from V_{OC} to J_{SC}) at different scanning speeds (B, backward; F, forward).

Table S2. Photovoltaic parameters for the stability of PSCs measured under AM 1.5 G illumination (solar cells were sealed with epoxy and stored in a dessicator).

Table S3. Composition of perovskite composite film determined by Rietveld refinement.

REFERENCES AND NOTES

1. M. Grätzel, The light and shade of perovskite solar cells. *Nat. Mater.* **13**, 838–842 (2014).
2. A. Kojima, K. Teshima, Y. Shirai, T. Miyasaka, Organometal halide perovskites as visible-light sensitizers for photovoltaic cells. *J. Am. Chem. Soc.* **131**, 6050–6051 (2009).
3. J.-H. Im, C.-R. Lee, J.-W. Lee, S.-W. Park, N.-G. Park, 6.5% efficient perovskite quantum-dot-sensitized solar cell. *Nanoscale* **3**, 4088–4093 (2011).
4. I. Chung, B. Lee, J. He, R. P. H. Chang, M. G. Kanatzidis, All-solid-state dye-sensitized solar cells with high efficiency. *Nature* **485**, 486–489 (2012).
5. H.-S. Kim, C.-R. Lee, J.-H. Im, K.-B. Lee, T. Moehl, A. Marchioro, S.-J. Moon, R. Humphry-Baker, J.-H. Yum, J. E. Moser, M. Grätzel, N.-G. Park, Lead iodide perovskite sensitized all-solid-state submicron thin film mesoscopic solar cell with efficiency exceeding 9%. *Sci. Rep.* **2**, 591 (2012).
6. M. M. Lee, J. Teuscher, T. Miyasaka, T. N. Murakami, H. J. Snaith, Efficient hybrid solar cells based on meso-superstructured organometal halide perovskites. *Science* **338**, 643–647 (2012).
7. J. Burschka, N. Pellet, S.-J. Moon, R. Humphry-Baker, P. Gao, M. K. Nazeeruddin, M. Grätzel, Sequential deposition as a route to high-performance perovskite-sensitized solar cells. *Nature* **499**, 316–319 (2013).
8. W. S. Yang, J. H. Noh, N. J. Jeon, Y. C. Kim, S. Ryu, J. Seo, S. I. Seok, High-performance photovoltaic perovskite layers fabricated through intramolecular exchange. *Science* **348**, 1234–1237 (2015).
9. N. Pellet, P. Gao, G. Gregori, T.-Y. Yang, M. K. Nazeeruddin, J. Maier, M. Grätzel, Mixed-organic-cation perovskite photovoltaics for enhanced solar-light harvesting. *Angew. Chem. Int. Ed.* **53**, 3151–3157 (2014).
10. N. J. Jeon, J. H. Noh, W. S. Yang, Y. C. Kim, S. Ryu, J. Seo, S. I. Seok, Compositional engineering of perovskite materials for high-performance solar cells. *Nature* **517**, 476–480 (2015).
11. W. Tress, N. Marinova, O. Inganäs, M. K. Nazeeruddin, S. M. Zakeeruddin, M. Graetzel, Predicting the open-circuit voltage of $CH_3NH_3PbI_3$ perovskite solar cells using electroluminescence and photovoltaic quantum efficiency spectra: The role of radiative and non-radiative recombination. *Adv. Energy Mater.* **5**, 1400812 (2015).
12. L. Gil-Escrig, G. Longo, A. Pertegás, C. Roldán-Carmona, A. Soriano, M. Sessolo, H. J. Bolink, Efficient photovoltaic and electroluminescent perovskite devices. *Chem. Commun.* **51**, 569–571 (2015).
13. Y. Shao, Z. Xiao, C. Bi, Y. Yuan, J. Huang, Origin and elimination of photocurrent hysteresis by fullerene passivation in $CH_3NH_3PbI_3$ planar heterojunction solar cells. *Nat. Commun.* **5**, 5784 (2014).
14. Z. Ren, A. Ng, Q. Shen, H. C. Gokkaya, J. Wang, L. Yang, W.-K. Yiu, G. Bai, A. B. Djurišić, W. W.-F. Leung, J. Hao, W. K. Chan, C. Surya, Thermal assisted oxygen annealing for high efficiency planar $CH_3NH_3PbI_3$ perovskite solar cells. *Sci. Rep.* **4**, 6752 (2014).
15. Q. Chen, H. Zhou, T.-B. Song, S. Luo, Z. Hong, H.-S. Duan, L. Dou, Y. Liu, Y. Yang, Controllable self-induced passivation of hybrid lead iodide perovskites toward high performance solar cells. *Nano Lett.* **14**, 4158–4163 (2014).
16. T. Supasai, N. Rujisamphan, K. Ullrich, A. Chemseddine, T. Dittrich, Formation of a passivating $CH_3NH_3PbI_3$/PbI_2 interface during moderate heating of $CH_3NH_3PbI_3$ layers. *Appl. Phys. Lett.* **103**, 183906 (2013).
17. L. Wang, C. McCleese, A. Kovalsky, Y. Zhao, C. Burda, Femtosecond time-resolved transient absorption spectroscopy of $CH_3NH_3PbI_3$ perovskite films: Evidence for passivation effect of PbI_2. *J. Am. Chem. Soc.* **136**, 12205–12208 (2014).
18. V. Somsongkul, F. Lang, A. R. Jeong, M. Rusu, M. Arunchaiya, T. Dittrich, Hole blocking PbI_2/$CH_3NH_3PbI_3$ interface. *Phys. Status Solidi* **8**, 763–766 (2014).

19. D. H. Cao, C. C. Stoumpos, C. D. Malliakas, M. J. Katz, O. K. Farha, J. T. Hupp, M. G. Kanatzidis, Remnant PbI_2, an unforeseen necessity in high-efficiency hybrid perovskite-based solar cells? *APL Mater.* **2**, 091101 (2014).
20. S. Pathak, A. Sepe, A. Sadhanala, F. Deschler, A. Haghighirad, N. Sakai, K. C. Goedel, S. D. Stranks, N. Noel, M. Price, S. Hüttner, N. A. Hawkins, R. H. Friend, U. Steiner, H. J. Snaith, Atmospheric influence upon crystallization and electronic disorder and its impact on the photophysical properties of organic-inorganic perovskite solar cells. *ACS Nano* **9**, 2311–2320 (2015).
21. H. J. Snaith, A. Abate, J. M. Ball, G. E. Eperon, T. Leijtens, N. K. Noel, S. D. Stranks, J. T.-W. Wang, K. Wojciechowski, W. Zhang, Anomalous hysteresis in perovskite solar cells. *J. Phys. Chem. Lett.* **5**, 1511–1515 (2014).
22. E. T. Hoke, K. Vandewal, J. A. Bartelt, W. R. Mateker, J. D. Douglas, R. Noriega, K. R. Graham, J. M. J. Fréchet, A. Salleo, M. D. McGehee, Recombination in polymer:fullerene solar cells with open-circuit voltages approaching and exceeding 1.0 V. *Adv. Energy Mater.* **3**, 220–230 (2013).
23. D. Di Nuzzo, G.-J. A. H. Wetzelaer, R. K. M. Bouwer, V. S. Gevaerts, S. C. J. Meskers, J. C. Hummelen, P. W. M. Blom, R. A. J. Janssen, Simultaneous open-circuit voltage enhancement and short-circuit current loss in polymer: Fullerene solar cells correlated by reduced quantum efficiency for photoinduced electron transfer. *Adv. Energy Mater.* **3**, 85–94 (2013).
24. N. Marinova, W. Tress, R. Humphry-Baker, M. I. Dar, V. Bojinov, S. M. Zakeeruddin, M. K. Nazeeruddin, M. Grätzel, Light harvesting and charge recombination in $CH_3NH_3PbI_3$ perovskite solar cells studied by hole transport layer thickness variation. *ACS Nano* **9**, 4200–4209 (2015).
25. K. Vandewal, K. Tvingstedt, A. Gadisa, O. Inganäs, J. V. Manca, On the origin of the open-circuit voltage of polymer-fullerene solar cells. *Nat. Mater.* **8**, 904–909 (2009).
26. T. Kirchartz, A. Helbig, W. Reetz, M. Reuter, J. H. Werner, U. Rau, Reciprocity between electroluminescence and quantum efficiency used for the characterization of silicon solar cells. *Prog. Photovolt. Res. Appl.* **17**, 394–402 (2009).
27. Z.-K. Tan, R. S. Moghaddam, M. L. Lai, P. Docampo, R. Higler, F. Deschler, M. Price, A. Sadhanala, L. M. Pazos, D. Credgington, F. Hanusch, T. Bein, H. J. Snaith, R. H. Friend, Bright light-emitting diodes based on organometal halide perovskite. *Nat. Nanotechnol.* **9**, 687–692 (2014).
28. O. A. Jaramillo-Quintero, R. S. Sanchez, M. Rincon, I. Mora-Sero, Bright visible-infrared light emitting diodes based on hybrid halide perovskite with Spiro-OMeTAD as a hole-injecting layer. *J. Phys. Chem. Lett.* **6**, 1883–1890 (2015).
29. J. Wang, N. Wang, Y. Jin, J. Si, Z.-K. Tan, H. Du, L. Cheng, X. Dai, S. Bai, H. He, Z. Ye, M. L. Lai, R. H. Friend, W. Huang, Interfacial control toward efficient and low-voltage perovskite light-emitting diodes. *Adv. Mater.* **27**, 2311–2316 (2015).
30. G. Giorgi, J.-I. Fujisawa, H. Segawa, K. Yamashita, Small photocarrier effective masses featuring ambipolar transport in methylammonium lead iodide perovskite: A density functional analysis. *J. Phys. Chem. Lett.* **4**, 4213–4216 (2013).

Acknowledgments: We thank A. Wakamiya (Institute for Chemical Research, Kyoto University, Uji, Kyoto 611-0011, Japan) for providing purified PbI_2. **Funding:** This work was supported by the European Union Seventh Framework Program (FP7/2007-2013) under grant agreement 604032 (ENERGY.2012.10.2.1) of the MESO project (FP7/2007-2013) and under grant agreement 308997 (NANOMATCELL). M.G. gratefully acknowledges financial support from SNSF-NanoTera (SYNERGY), the Swiss Federal Office of Energy (SYNERGY), CCEM-CH in the 9th call proposal 906: CONNECT PV, the SNSF NRP70 "Energy Turnaround," and the GRAPHENE project supported by the European Commission Seventh Framework Program (under contract 604391). M.I.D. thanks the European Community's Seventh Framework Program (FP7/2007-2013) under grant agreement 281063 of the Powerweave project. A.A. and J.L. received funding from the European Union's Seventh Framework Program for research, technological development, and demonstration under grant agreement 291771. **Author contributions:** D.B. designed and carried out the experimental study on device fabrication and basic characterization. W.T. performed optoelectronic measurements, analyzed and interpreted the data, and wrote the manuscript together with P.G., M.G., A.H., and D.B. XRD measurements and analyses were performed by P.G., K.S., and M.I.D., whereas J.L. performed SEM measurements. M.I.D. performed PL measurements. C.R. performed optoelectronic characterization. A.A., F.G., and J.-P.C.B. developed the basic recipe for the perovskite deposition. J.-D.D. was responsible for the certification. S.M.Z. and M.K.N. coordinated the research, whereas A.H. and M.G. supervised the project. **Competing interests:** The authors declare that they have no competing interests. **Data and materials availability:** All data needed to evaluate the conclusions in the paper are present in the paper and/or in the Supplementary Materials. Additional data are available from D.B. (dongqin.bi@epfl.ch) upon request.

Submitted 26 August 2015
Accepted 6 November 2015
Published 1 January 2016
10.1126/sciadv.1501170

Citation: D. Bi, W. Tress, M. I. Dar, P. Gao, J. Luo, C. Renevier, K. Schenk, A. Abate, F. Giordano, J.-P. Correa Baena, J.-D. Decoppet, S. M. Zakeeruddin, M. K. Nazeeruddin, M. Grätzel, A. Hagfeldt, Efficient luminescent solar cells based on tailored mixed-cation perovskites. *Sci. Adv.* **2**, e1501170 (2016).

Science Advances

Efficient luminescent solar cells based on tailored mixed-cation perovskites

Dongqin Bi, Wolfgang Tress, M. Ibrahim Dar, Peng Gao, Jingshan Luo, Clémentine Renevier, Kurt Schenk, Antonio Abate, Fabrizio Giordano, Juan-Pablo Correa Baena, Jean-David Decoppet, Shaik Mohammed Zakeeruddin, Mohammad Khaja Nazeeruddin, Michael Grätzel and Anders Hagfeldt

Sci Adv **2** (1), e1501170.
DOI: 10.1126/sciadv.1501170